Small-Signal Analysis in Two Calculation Sections and Experimental Validation of Up-Converted Coherent Population Oscillations in Semiconductor Optical Amplifiers

Noor Hamdash, Ammar Sharaiha, Thierry Rampone, Denis Le Berre, Noham Martin, and Cédric Quendo

***Abstract*—This paper presents theoretical and experimental analysis of up-converted coherent population oscillations (Up-CPO) in semiconductor optical amplifiers (SOAs) for tunable optical phase shift applications at high frequencies. The study of Up-CPO frequency response is carried out by a small-signal analysis of a SOA modeled by two calculation sections in order to better take into account the nonlinear effects such as the SOA gain saturation. We demonstrate that we can fully determine the dynamic parameters of Up-CPO from the experimental frequency response of an optical probe signal obtained by cross-gain modulation mechanism. The Up-CPO frequency responses are measured for three SOAs with different cut-off frequencies up to 18.45 GHz. We finally validate experimentally the obtained analytical frequency responses for the three SOAs over different operating points, each characterized by the corresponding optical gain.**

***Index Terms*—Semiconductor optical amplifier (SOA), slow/fast light (SFL), small-signal modeling, up-converted CPO (Up-CPO), microwave phase shifter, microwave photonics (MWP), cross-gain modulation (XGM).**

I. Introduction

MICROWAVE photonics (MWP), which combines radiofrequency and optoelectronics domains, has attracted a great deal of interest over the past years. The generation and processing of microwave and mm-wave signals by optical means allow to exploit the advantages of photonics, such as low loss, high bandwidth and immunity to electromagnetic interferences [1]. MWP is a key technology to enable the realization of frequency conversion, reconfigurable filtering, phase shifting and true time delaying functions [1]–[3].

Manuscript received March 18, 2021; revised June 9, 2021; accepted June 14, 2021. Date of publication June 23, 2021; date of current version July 13, 2021. *(Corresponding author: Thierry Rampone.)*

Noor Hamdash is with the Lab-STICC UMR CNRS 6285, Université de Bretagne Occidentale, 29200 Brest, France, and also with the Lab-STICC UMR CNRS 6285, École Nationale d'Ingénieurs de Brest, Technopôle Brest-Iroise, 29238 Brest, France (e-mail: hamdash@enib.fr).

Ammar Sharaiha and Thierry Rampone are with the Lab-STICC UMR CNRS 6285, École Nationale d'Ingénieurs de Brest, Technopôle Brest-Iroise, 29238 Brest, France (e-mail: sharaiha@enib.fr; rampone@enib.fr).

Denis Le Berre, Noham Martin, and Cédric Quendo are with the Lab-STICC UMR CNRS 6285, Université de Bretagne Occidentale, 29200 Brest, France (e-mail: denis.le-berre@univ-brest.fr; noham.martin@univ-brest.fr; cedric.quendo@univ-brest.fr).

Digital Object Identifier 10.1109/JPHOT.2021.3090209

The generation of tunable optical phase shifts and delay lines which must be continuously tunable for some applications, such as phased-array antenna (PAA) [1], is a key functionality in MWP [2]. One of the most promising methods to control the speed of light [4]–[6] is based on coherent population oscillations (CPO) in semiconductor optical amplifiers (SOA). It provides a continuously tunable microwave photonic phase shifter, which is the fundamental part used in PAA to perform photonic true time delay (TTD) in beamforming antennas [7]. True time delays are needed to obtain wide instantaneous bandwidth and beam squint-free operation of the PAA [3]. Tunable microwave photonic phase shifter can be implemented by properly profiting from self-gain modulation (SGM) and cross-gain modulation (XGM) in semiconductor waveguides [8]–[9].

SOAs have been used as a freestanding device for MWP phase shifters and several works have covered tunable phase shifting based on CPO effects in SOA [5]–[15]. However, CPO techniques limit the operating frequency applications to few hundreds of GHz due to the SOA carrier lifetime [7] [11], when used for the generation of a time delay. Nevertheless, it has been demonstrated that the integrated phase shift or time delay generator based on frequency up-converted CPO in a SOA, noted by Up-CPO, eliminates the issue of the intrinsic limitation of the carrier lifetime, leading to the generation of a phase shift or a time delay on signals up to THz [11]. The data-signal has a low bandwidth modulated onto the carrier-wave below a few GHz, due to XGM mechanisms. However, the Up-CPO enables the extension of the operating frequency of a tunable phase shift/delay line based on CPO effects in SOA from a few GHz up to THz. This is suitable for applications where the instantaneous bandwidth is limited to a few GHz, such as some radar applications.

The aim in this paper is to analyze, thanks to a small-signal modeling, the frequency response of Up-CPO and to validate experimentally the Up-CPO modeling by using three different types of SOAs considered as linear or nonlinear ones. For that purpose, we first describe the principle of Up-CPO in Section II, then we derive in Section III a small-signal analysis of the Up-CPO frequency response. In order to consider nonlinear effects in SOAs such as gain saturation, we subdivide the total SOA cavity length into two sections. The Up-CPO frequency response is then studied through the dynamic carrier lifetime

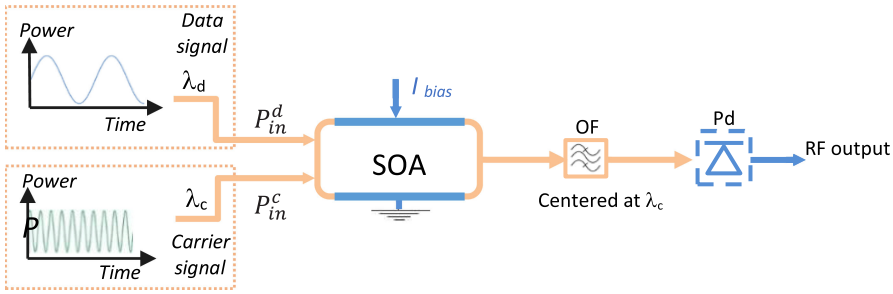

Fig. 1. Principle of Up-CPO. OF: Optical filter, Pd: Photodiode.

as a function of the injected optical powers. In Section IV, a comparison between theoretical data and experimental results on the amplitude and phase shift of the microwave signal is presented. The comparison concerns both a pump-probe and an Up-CPO implementation for three different types of SOAs, which is done for the first time, to the best of our knowledge. Conclusions are given in Section V.

II. Principle of Up-Converted CPO

Fig. 1 shows a schematic highlighting the fundamental concept of Up-CPO which combine CPO and XGM [11]. That is achieved by injecting two optical intensity-modulated signals into the SOA. A first optical signal P_{in}^{c} (carrier signal) at the wavelength λ_c is modulated at a high frequency (f_c), with f_c assumed to be larger than the inverse of the dynamic carrier density lifetime τ_d (i.e., $f_c >> 1/(2\pi\tau_d)$). Thus, the carrier density in the active region and the SOA optical gain are not affected by the modulation part of this signal at the high frequency f_c.

The second optical signal P_{in}^{d} (data signal) at the wavelength λ_d is modulated at a low frequency (f_d) with $f_d << 1/(2\pi\tau_d)$. Therefore, the carrier density oscillating at f_d leads to a dynamic variation of the optical gain. Thus, through XGM, the signal P_{in}^{c} is modulated by P_{in}^{d}, giving rise to signals at high frequencies $f_c \pm f_d$. In other words, the data signal at low frequency f_d is up-converted around the high frequency of the carrier, at $f_c \pm f_d$. After photodetection, the RF output signal provides information on the phase shift that can be tuned through the operating condition of the SOA [7], [11].

III. Small-Signal Analysis of Up-Converted CPO

The model used for small-signal analysis is based on a carrier density rate equation and a set of travelling-wave equations describing the amplified signal fields [4], [7], [11], [16]–[17]. We develop first in Section III-A the Up-CPO optical power response as a function of the SOA carrier density variation. In Section III-B, we show that the frequency responses of the carrier density can be extracted from the experimental results obtained in a pump-probe configuration in order to access to the Up-CPO frequency responses. The calculation is performed by dividing the SOA into 2 sections to better consider the SOA gain saturation. In Section III-C of this paragraph, we study the evolution of the dynamic carrier lifetimes as a function of the injected powers and finally in Section III-D we give the complete Up-CPO optical power response.

A. Up-CPO Optical Power Response as a Function of the SOA Mean Carrier Density

The optical power of data signal $P_{in}^{d}(t)$ and carrier signal $P_{in}^{c}(t)$ at the SOA input can be given by:

$$P_{in}^{x}\ (t) = \overline{P_{in}^{x}} + \frac{p_{in}^{x}}{2} e^{\,j\omega_x t} + \frac{p_{in}^{*x}}{2} e^{-j\omega_x t} \tag{1}$$

where the index x refers to carrier 'c' or data 'd' signal at the wavelength λ_x.$\overline{P_{in}^{x}}$ is the average optical input power at λ_x, p_{in}^{x} is the modulation part at the angular frequency ω_x of the optical signal at the wavelength λ_x and '$*$' stands for the complex conjugate value. By using a first-order Taylor expansion the input electrical field $E_{in}^{x}(t)$ corresponding to $P_{in}^{x}(t)$ can be written [18], considering its unit expressed in square root of Watt:

$$E_{in}^{x}(t) = \sqrt{P_{in}^{x}(t)}\ e^{j\Omega_x\, t} \approx \overline{E^x} \times \left(1 + \frac{p_{in}^{x}}{4\overline{P_{in}^{x}}} e^{j\omega_x t} + \frac{p_{in}^{*x}}{4\overline{P_{in}^{x}}} e^{-j\omega_x t}\right) \tag{2}$$

where $\overline{E^x} = \sqrt{\overline{P_{in}^{x}}}\ e^{j\Omega_x\, t}$ and Ω_x the angular frequency of the optical field at λ_x. We assume that the optical gains at λ_c and λ_d are identical, noted $\bar{G}$. At the SOA output, the optical field at the Up-CPO wavelength λ_c , can be obtained from:

$$E_{out}^{c}(t) = E_{in}^{c}(t)\sqrt{G(t)}e^{j\Delta\varphi} \tag{3}$$

where $\Delta\varphi$ is the difference of phase due to the propagation along the SOA.

The oscillation of the carrier density along the SOA length, inside the SOA active zone, is induced by the two input signals $P_{in}^{c}(t)$ and $P_{in}^{d}(t)$ at the angular frequencies ω_c and ω_d respectively. By considering a first-order approximation, the beating terms at $\omega_{c\pm d} = \omega_c \pm \omega_d$ can be neglected. By dividing the SOA in M calculation sections along its length, we can define a mean carrier density N_e which is the mean value of the carrier densities in the M sections, with $N_e = \sum_i \frac{N_i}{M}$ where N_i is the carrier density in section i. So, the expression of the mean carrier density $N_e(t)$ can be written as:

$$N_e(t) = \overline{N_e} + \frac{n_{e,\omega_d}}{2} e^{j\omega_d t} + \frac{n_{e,\omega_d}^{*}}{2} e^{-j\omega_d t} + \frac{n_{e,\omega_c}}{2} e^{j\omega_c t} + \frac{n_{e,\omega_c}^{*}}{2} e^{-j\omega_c t} \tag{4}$$

where $\overline{N_e}$ represents the static operating point and n_{e,ω_x} is the complex amplitude of the mean carrier density modulation at ω_x. Due to the cross-gain modulation (XGM), the SOA gain $G(t)$ at λ_c is modulated at the same pulsations as the carrier density around the static operating point $\bar{G}$. $\sqrt{G(t)}$ can be written, by using a first-order Taylor expansion, as:

$$\sqrt{G\left(t\right)} \sim \sqrt{\bar{G}}\left(1+\frac{\frac{\partial G}{\partial N}}{2\bar{G}}\left(\frac{n_{e,\omega_d}}{2}e^{j\omega_d t}+\frac{n^*_{e,\omega_d}}{2}e^{-j\omega_d t}+\frac{n_{e,\omega_c}}{2}e^{j\omega_c t}+\frac{n^*_{e,\omega_c}}{2}e^{-j\omega_c t}\right)\right) \tag{5}$$

Therefore, at λ_c, the complex amplitude terms of the Up-CPO signal output power at the pulsations ω_{c+d} and ω_{c-d} can be obtained by the quadratic detection of the terms calculated from (2), (3) and (5) as:

$$\begin{aligned} p^c_{out,\omega_{c+d}} &= \frac{p^c_{in}}{4}n_{e,\omega_d}\frac{\partial G}{\partial N}\left(1+\frac{\overline{P^c_{in}}}{p^c_{in}}n_{e,\omega_c}\frac{\partial G}{\partial N}\right) \\ &= \frac{p^c_{in}}{4}n_{e,\omega_d}\frac{\partial G}{\partial N}\left(1+\varepsilon_{c+d}\left(\omega_c\right)\right) \end{aligned} \tag{6}$$

$$\begin{aligned} p^c_{out,\omega_{c-d}} &= \frac{p^c_{in}}{4}\,n^*_{e,\omega_d}\frac{\partial G}{\partial N}\left(1+\frac{\overline{P^c_{in}}}{p^c_{in}}n^*_{e,\omega_c}\frac{\partial G}{\partial N}\right) \\ &= \frac{p^c_{in}}{4}\,n^*_{e,\omega_d}\frac{\partial G}{\partial N}\left(1+\varepsilon_{c-d}\left(\omega_c\right)\right) \end{aligned} \tag{7}$$

with $\varepsilon_{c+d}\left(\omega_c\right)=\frac{\overline{P^c_{in}}}{p^c_{in}}\,n_{e,\omega_c}\frac{\partial G}{\partial N}$ and $\varepsilon_{c-d}\left(\omega_c\right)=\frac{\overline{P^c_{in}}}{p^c_{in}}\,n^*_{e,\omega_c}\frac{\partial G}{\partial N}$. These two terms must be taken into account if f_c is close or below the cutoff frequency of $n_e(\omega)$. Usually, f_c is set significantly higher than the cutoff frequency of $n_e(\omega)$, thus the response in phase and amplitude of n_{e,ω_c} is negligible. It appears through (6) and (7) that the frequency response in amplitude and phase of the Up-CPO signals at ω_{c+d} and ω_{c-d} depends only on the frequency response of the mean carrier density oscillation due to the data signal through n_{e,ω_d} and n^*_{e,ω_d} respectively. Therefore, the Up-CPO frequency response in this case can be simplified as:

$$p^c_{out,\omega_{c+d}} \sim \frac{p^c_{in}}{4}n_{e,\omega_d}\frac{\partial G}{\partial N} \tag{8}$$

$$p^c_{out,\omega_{c-d}} \sim \frac{p^c_{in}}{4}n^*_{e,\omega_d}\frac{\partial G}{\partial N} \tag{9}$$

B. Small-Signal Frequency Response of the Carrier Density

Due to XGM in presence of the two input signals $P^c_{in}(t)$ and $P^d_{in}(t)$, as shown in (6) and (7), the Up-CPO frequency responses at $\omega_{c\pm d}$ are essentially related to the frequency response of the carrier density of the data signal, n_{e,ω_d}. To access experimentally to the frequency response of n_{e,ω_d} due to XGM, without the oscillation of $P^c_{in}(t)$, a pump-probe setup is used. In this case, $P^c_{in}(t)$ is set as a continuous-wave signal and used as a probe noted $\overline{P^{Pr}_{in}}$, and $P^d_{in}(t)$ is considered as the pump, a time varying signal noted $P^{Pu}_{in}(t)$.

Generally, in small-signal analysis, the SOA is modeled by only one calculation section [4], [5], [10]–[14]. In order to better take into account the nonlinear effect due to the gain saturation, the model must include an extra number of sections, but causing the analytical expression of $n_e()$ to become much more complex. As we increase the number of sections, so does the complexity of the equation; thus, we divide the total SOA length into only two sections of equal lengths ($L_1 = L_2 = L/2$). Each section is biased by half of the total SOA bias current I ($I_1 = I_2 = I/2$) (Fig. 2).

Therefore, in the pump-probe configuration, an intensity-modulated optical power acting as a pump signal at λ_{Pu} is injected in the first SOA section at the SOA input (Fig. 2), which is expressed at the SOA input by:

$$P^{Pu}_{in}\left(t\right)=P^{Pu}_{in,1}\ \left(t\right)=\overline{P^{Pu}_{in}}+\frac{p^{Pu}_{in}}{2}e^{\,j\omega_{Pu}t}+\frac{p^{*Pu}_{in}}{2}e^{-j\omega_{Pu}t} \tag{10}$$

where $\overline{P^{Pu}_{in}}$ is the average optical input power at λ_{Pu}, p^{Pu}_{in} is the modulation part at the angular frequency ω_{Pu} of the optical signal at wavelength λ_{Pu} and '$*$' stands for the complex conjugate value. A second signal, a continuous-wave power acting as a probe signal $P^{Pr}_{in1}(t)=\overline{P^{Pr}_{in}}$ at λ_{Pr} is injected simultaneously at the SOA input (Fig. 2). The SOA carrier densities are respectively noted N_i in section i, with $i = 1$ or 2. We assume that the SOA gains at λ_{Pu} and λ_{Pr} are the same: for the section i we have $\overline{G^{Pu}_i}=\overline{G^{Pr}_i}=\overline{G_i}$.

The amplification of $P^{Pu}_{in,1}$ induces a modulation of the carrier density and then of the SOA gain at the angular frequency ω_{Pu}. N_i and G_i can be written in section i by:

$$N_i\left(t\right)=\overline{N_i}+\frac{n_{i,\omega_{Pu}}}{2}e^{j\omega_{Pu}t}+\frac{n^*_{i,\omega_{Pu}}}{2}e^{-j\omega_{Pu}t} \tag{11}$$

$$G_i\left(t\right)=\overline{G_i}+\frac{n_{i,\omega_{Pu}}}{2}\frac{\partial G_i}{\partial N_i}e^{j\omega_{Pu}t}+\frac{n^*_{i,\omega_{Pu}}}{2}\frac{\partial G_i}{\partial N_i}e^{-j\omega_{Pu}t} \tag{12}$$

$\overline{N_i}$ and $\overline{G_i}$ represent the static operating point in each section. $n_{i,\omega_{Pu}}$ is the complex amplitude of the carrier density modulation in section i at ω_{Pu}, $n^*_{i,\omega_{Pu}}$ is the complex conjugate of $n_{i,\omega_{Pu}}$.

The dynamics of CPO are governed by the carrier density rate equation. The general form of the rate equation, in section i, can be written as [16]–[17] by:

$$\frac{dN_i}{dt}=\frac{I_i}{qV}-R_{nr,i}-R_{ASE,i}-R_{st,i} \tag{13}$$

where q is the elementary charge, V is the optical active zone volume of length *L/2*, width w and height d. $R_{nr,i}$, $R_{ASE,i}$ and $R_{st,i}$ are respectively the non-radiative, the ASE and the stimulated recombination rates. The influence of $R_{nr,i}$ and $R_{ASE,i}$ can be taken into account by $N_i/\tau_{e,i}$, where $\tau_{e,i}$ is the effective carrier lifetime calculated from the carrier lifetimes τ_i, due to $R_{nr,i}$, and $\tau_{ase,i}$, due to $R_{ASE,i}$, with $\frac{1}{\tau_{e,i}}=\frac{1}{\tau_i}+\frac{1}{\tau_{ase,i}}$ [19]–[20].

The recombination rate $R_{st,i}$ due to the amplification of the optical pump and probe signals at wavelengths λ_{Pr} and λ_{Pu}, can be given in both sections by the following equation [16]:

$$R_{st,i}=\frac{2}{\Gamma aL\tau_{e,i}}\left(\frac{P^{Pu}_{in,i}\left(t\right)\left(G_i-1\right)}{P^{Pu}_{sat,\mathrm{i}}}+\frac{\overline{P^{Pr}_{in,i}}\left(G_i-1\right)}{P^{Pr}_{sat,\mathrm{i}}}\right) \tag{14}$$

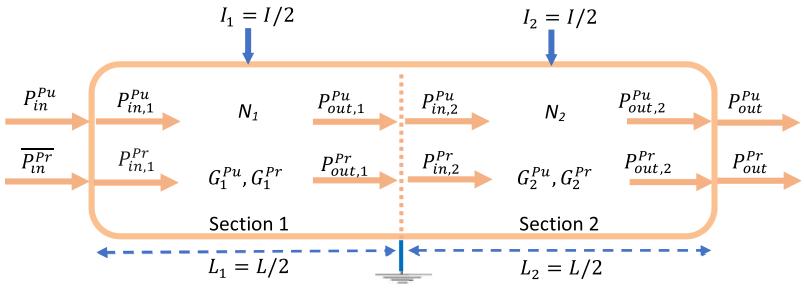

Fig. 2. Principle of SOA modeling by two calculation sections in presence of an intensity-modulated pump signal $P_{in}^{Pu}(t)$ at λ_{Pu} and a continuous-wave probe signal $\overline{P_{in}^{Pr}}$ at λ_{Pr}.

where $P_{sat,\mathrm{i}}^{Pu} = \frac{wdW_p^{Pu}}{\Gamma a \tau_{e,i}}$ is the material saturation power at λ_{Pu}, $P_{sat,\mathrm{i}}^{Pr} = \frac{wdW_p^{Pr}}{\Gamma a \tau_{e,i}}$ is the material saturation power at λ_{Pr}, W_p^{Pu} and W_p^{Pr} are the photon energy at the signal wavelength λ_{Pu} and λ_{Pr}, respectively. Γ is the optical confinement factor in the active zone, a is the peak-gain coefficient.

The optical gain of the SOA as well as the partial derivative of the gain with respect to the carrier density are given by:

$$G_i\left(N_i\right) = e^{\Gamma a(N_i - N_0)L_i} \tag{15}$$

$$\frac{\partial G_i}{\partial N_i} = \Gamma a L_i \overline{G_i} \tag{16}$$

with N_0 the carrier density at transparency.

1) Carrier Density Modulation in the First Section: By introducing (14) into (13), the rate equation for the first section is

$$\frac{dN_1}{dt} = \frac{I_1}{qV} - \frac{N_1}{\tau_{e,1}} - \frac{P_{in,1}^{Pu}(t)\left(G_1 - 1\right)}{\Gamma a L_1 \tau_{e,1} P_{sat,1}^{Pu}} - \frac{\overline{P_{in,1}^{Pr}}\left(G_1 - 1\right)}{\Gamma a L_1 \tau_{e,1} P_{sat,1}^{Pr}} \tag{17}$$

The complex amplitude of the carrier density modulation $n_{1,\omega_{Pu}}$ (18) is given by small-signal modeling using (10)–(12), and by applying the derivative of (17). We consider first order modulation terms, and substitute (16) into the derivative of (17).

$$n_{1,\omega_{Pu}} = -\frac{1}{\Gamma a\, L_1 \left(1 + K_1^{Pu}\right) P_{sat,1}^{Pu}} \left(\frac{\overline{G_1} - 1}{1 + j\omega\tau_{d,1}}\right) p_{in,1}^{Pu} \tag{18}$$

where $\tau_{d,1} = \frac{\tau_{e,1}}{1+K_1^{Pu}}$ is the dynamic carrier lifetime in the first section and $K_1^{Pu} = \frac{\overline{P_{in,1}^{Pu}}}{P_{sat,1}^{Pu}}\ \overline{G_1}$.

2) Carrier Density Modulation in the Second Section: The input powers of the second section depends on the output powers of Section I, where $P_{out,1}^{Pu}(t) = P_{in,2}^{Pu}(t) = P_{in,1}^{Pu}(t)G_1(t)$ and $P_{out,1}^{Pr}(t) = P_{in,2}^{Pr}(t) = \overline{P_{in,1}^{Pr}}G_1(t)$. So, for $i = 2$, the rate equation for the second section is given as:

$$\frac{dN_2}{dt} = \frac{I_2}{qV} - \frac{N_2}{\tau_{e,2}} - \frac{P_{in,2}^{Pu}(t)\left(G_2 - 1\right)}{\Gamma a L_2 \tau_{e,2} P_{sat,2}^{Pu}} - \frac{P_{in,2}^{Pr}(t)\left(G_2 - 1\right)}{\Gamma a L_2 \tau_{e,2} P_{sat,2}^{Pr}} \tag{19}$$

The complex amplitude of the carrier density modulation $n_{2,\omega_{Pu}}$ in the second section can be calculated as in (20) by small-signal modeling using (10)–(12), and by applying the derivative of (19). We consider first order modulation terms, and substitute (16) into the derivative of (19).

$$n_{2,\omega_{Pu}} = -\frac{1}{\Gamma a L_2 \left(1 + K_2^{Pr} + K_2^{Pu}\right) P_{sat,2}^{Pu}} \left(\frac{\overline{G_2} - 1}{1 + j\omega\tau_{d,2}}\right) \times \left(p_{in,1}^{Pu}\overline{G_1} + \overline{P_{in,1}^{Pu}} n_{1,\omega_{Pu}} \frac{\partial G_1}{\partial N_1} + \overline{P_{in,1}^{Pr}} n_{1,\omega_{Pu}} \frac{\partial G_1}{\partial N_1}\right) \tag{20}$$

where $\tau_{d,2} = \frac{\tau_{e,2}}{1+K_2^{Pr}+K_2^{Pu}}$ is the dynamic carrier lifetime in the second section, $K_2^{Pu} = \frac{\overline{P_{in,1}^{Pu}}}{P_{sat,2}^{Pu}}\bar{G}$ and $\bar{G} = \overline{G_1}\ \overline{G_2}$.

The probe and pump optical powers at the input of the second section can be written respectively from (10) and (12) by considering first-order terms as:

$$P_{in,2}^{Pr}(t) = \overline{P_{in,1}^{Pr}}\,\overline{G_1} + \overline{P_{in,1}^{Pr}} \frac{n_{1,\omega_{Pu}}}{2} \frac{\partial G_1}{\partial N_1} e^{j\omega_{Pu}t} + \overline{P_{in,1}^{Pr}} \frac{n_{1,\omega_{Pu}}^*}{2} \frac{\partial G_1}{\partial N_1} e^{-j\omega_{Pu}t} \tag{21}$$

$$P_{in,2}^{Pu}(t) = \overline{P_{in,1}^{Pu}}\overline{G_1} + \left(\frac{p_{in,1}^{Pu}}{2}\overline{G_1} + \overline{P_{in,1}^{Pu}} \frac{n_{1,\omega_{Pu}}}{2} \frac{\partial G_1}{\partial N_1}\right) e^{j\omega_{Pu}t} + \left(\frac{p_{in,1}^{*Pu}}{2}\overline{G_1} + \overline{P_{in,1}^{Pu}} \frac{n_{1,\omega_{Pu}}^*}{2} \frac{\partial G_1}{\partial N_1}\right) e^{-j\omega_{Pu}t} \tag{22}$$

3) Probe Output Power: At the SOA output, the complex amplitude of the probe signal at $\pm\omega_{Pu}$ can be given from (10) and (12) by considering the first order terms as:

$$p_{out,\omega_{Pu}}^{Pr} = \overline{P_{in,1}^{Pr}}\,\overline{G_2} \frac{n_{1,\omega_{Pu}}}{2} \frac{\partial G_1}{\partial N_1} + \overline{P_{in,1}^{Pr}}\,\overline{G_1} \frac{n_{2,\omega_{Pu}}}{2} \frac{\partial G_2}{\partial N_2} \tag{23}$$

$$p_{out,-\omega_{Pu}}^{Pr} = \overline{P_{in,1}^{Pr}}\ \overline{G_2} \frac{n_{1,\omega_{Pu}}^*}{2} \frac{\partial G_1}{\partial N_1} + \overline{P_{in,1}^{Pr}}\,\overline{G_1} \frac{n_{2,\omega_{Pu}}^*}{2} \frac{\partial G_2}{\partial N_2} \tag{24}$$

Then, by using (16), we express $p_{out,\pm\omega_{Pu}}^{Pr}$ as a function of the mean carrier density as:

$$p_{out,\omega_{Pu}}^{Pr} = \overline{P_{in,1}^{Pr}}\overline{G_1 G_2}\Gamma a \frac{L}{2} \frac{n_{1,\omega_{Pu}}}{2} + \overline{P_{in,1}^{Pr}}\overline{G_1 G_2}\Gamma a \frac{L}{2} \frac{n_{2,\omega_{Pu}}}{2}$$

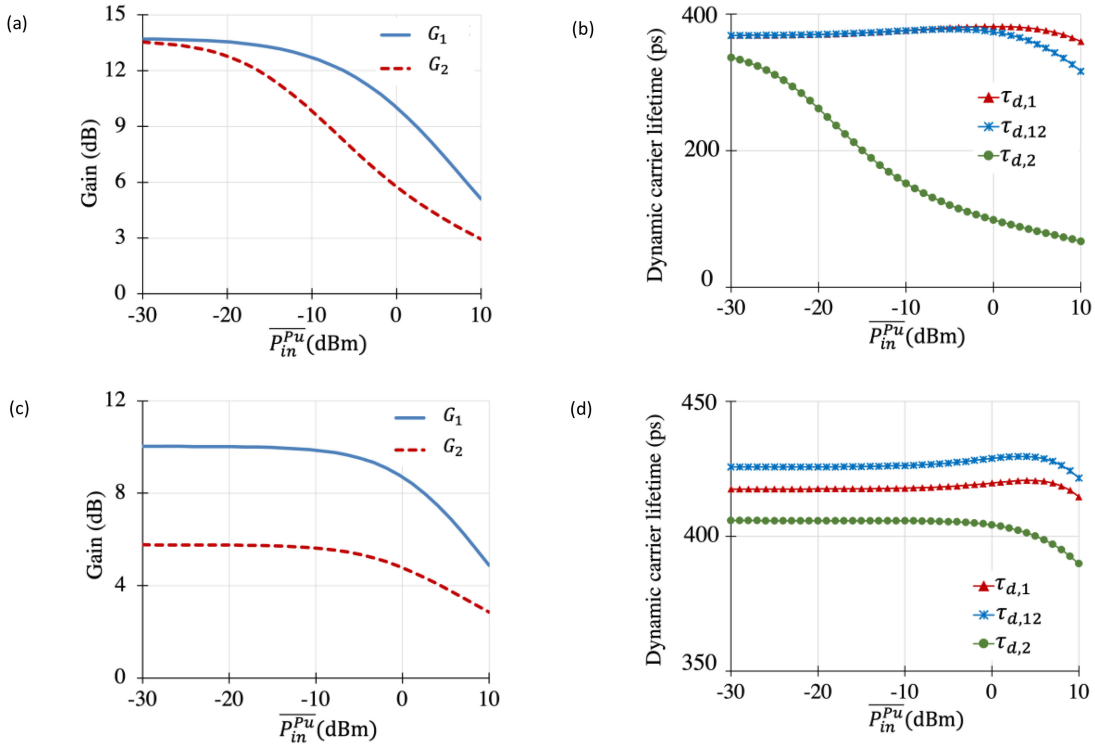

Fig. 3. Gain for Sections 1 and 2 for : $\overline{P_{in}^{Pr}} = -30$ dBm (a), $\overline{P_{in}^{Pr}} = 0$ dBm (c). Dynamic carrier lifetime for: $\overline{P_{in}^{Pr}} = -30$ dBm (b), $\overline{P_{in}^{Pr}} = 0$ dBm (d).

$$= \overline{P_{in,1}^{Pr}}\,\bar{G}\Gamma aL\frac{n_{e,\omega_{Pu}}}{2} \tag{25}$$

$$p_{out,-\omega_{Pu}}^{Pr} = \overline{P_{in,1}^{Pr}}\bar{G}\Gamma aL\frac{n_{e,\omega_{Pu}}^{*}}{2} \tag{26}$$

with $n_{e,\omega_{Pu}} = \frac{n_{1,\omega_{Pu}}+n_{2,\omega_{Pu}}}{2}$ and $n_{e,\omega_{Pu}}^{*} = \frac{n_{1,\omega_{Pu}}^{*}+n_{2,\omega_{Pu}}^{*}}{2}$ equivalent to the mean value of the complex amplitude of the carrier density.

Thereby, Eq. (25) and (26) show that a pump-probe setup can provide access to the frequency response of the carrier density, which will be used to analyze the Up-CPO frequency response defined in (8) and (9). By substituting (18) and (20) into (25) and (26) we obtain the expression of $p_{out,\pm\omega_{Pu}}^{Pr}$, $n_{e,\omega_{Pu}}$ and $n_{e,\omega_{Pu}}^{*}$:

$$p_{out,\pm\omega_{Pu}}^{Pr} = -\frac{K_{n1n2}\overline{P_{in,1}^{Pr}}\bar{G}}{2P_{sat,1}^{Pu}P_{sat,2}^{Pu}} \times\left(\frac{1\pm j\omega\tau_{d,12}}{(1\pm j\omega\tau_{d,1})(1\pm j\omega\tau_{d,2})}\right)p_{in,1}^{Pu} \tag{27}$$

$$n_{e,\omega_{Pu}} = -\frac{K_{n1n2}}{\Gamma aLP_{sat,1}^{Pu}P_{sat,2}^{Pu}} \times\left(\frac{1+j\omega\tau_{d,12}}{(1+j\omega\tau_{d,1})(1+j\omega\tau_{d,2})}\right)p_{in,1}^{Pu} \tag{28}$$

$$n_{e,\omega_{Pu}}^{*} = -\frac{K_{n1n2}}{\Gamma aLP_{sat,1}^{Pu}P_{sat,2}^{Pu}} \times\left(\frac{1-j\omega\tau_{d,12}}{(1-j\omega\tau_{d,1})(1-j\omega\tau_{d,2})}\right)p_{in,1}^{Pu} \tag{29}$$

with $\tau_{d,12} = \left(\frac{K_{n2}\overline{G_1}\tau_{d,1}P_{sat,1}^{Pu}+K_{n1}\tau_{d,2}P_{sat,2}^{Pu}}{K_{n1n2}}\right)$, $K_{n1n2} = P_{sat,2}^{Pu}K_{n1} + K_{n2}\overline{G_1}P_{sat,1}^{Pu}\left(1-K_{n1}\left(\frac{\overline{P_{in,1}^{Pr}}+\overline{P_{in,1}^{Pu}}}{P_{sat,1}^{Pu}}\right)\right)$, $K_{n1} = \frac{\overline{G_1}-1}{(1+K_1^{Pu})}$, and $K_{n2} = \frac{\overline{G_2}-1}{(1+K_2^{Pu}+K_2^{Pr})}$.

C. Evaluation of Dynamic Carrier Lifetime

As the frequency response of $p_{out,\pm\omega_{Pu}}^{Pr}$ in (27) depends on the dynamic carrier lifetimes $\tau_{d,12}$, $\tau_{d,1}$ and $\tau_{d,2}$, we analyze in this paragraph their evolution as a function of the injected powers $\overline{P_{in}^{Pr}}$ and $\overline{P_{in}^{Pu}}$. The calculation of $\tau_{d,12}$, $\tau_{d,1}$ and $\tau_{d,2}$ is done after resolving the rate equations (17) and (19) by using 2 calculation sections for the SOA presented in [16]. We consider two cases where the probe input power $\overline{P_{in}^{Pr}}$ is set first at a low power (-30 dBm) and then at a high power to saturate the SOA (0 dBm). For each case, we vary the pump input power $\overline{P_{in}^{Pu}}$ from -30 to 10 dBm. Fig. 3(a) and 3(c) depict the gain evolution versus the pump input optical power for $\overline{P_{in}^{Pr}} = -30$ dBm and 0 dBm, respectively. We deduce from these two figures $P_{sat,1}^{Pu}$ and $P_{sat,2}^{Pu}$, where $P_{sat,i}^{Pu} = \frac{\overline{P_{out,i}}|_{-3\,dB}}{ln(2)}$ [21], with $\overline{P_{out,i}}|_{-3\,dB}$ the optical output power in section i for the optical gain reduced by -3 dB.

As seen in Fig. 3(b) and 3(d), $\tau_{d,1}$ is always greater than $\tau_{d,2}$. When the optical gain in each section is nearly unsaturated, corresponding to $\overline{P_{in}^{Pu}}$ lower than -10 dBm and $\overline{P_{in}^{Pr}}$ set at -30 dBm, Fig. 3(b) shows that $\tau_{d,12} \sim \tau_{d,1}$. In this case, (27) tends to a first-order low-pass response. This indicates that modeling the SOA by only one section is sufficient.

TABLE I
STATIC CHARACTERISTICS OF THE THREE SOAS

	SOA-L	SOA-NL	SOA-XN
Unsaturated gain (dB)	18.8	30.8	30.5
$P_{out}\vert_{-3\ dB}$ (dBm)	12.6 (at 300 mA)	13.8 (at 300 mA)	14.5 (at 400 mA)

For higher $\overline{P_{in}^{Pu}}$, G_2 is more saturated than G_1, this in turn leads to $\tau_{d,12} < \tau_{d,1}$ as shown in Fig. 3(b). A deep saturation, for the case where $\overline{P_{in}^{Pr}}$ is set at 0 dBm, leads to always have $\tau_{d,12} > \tau_{d,1}$ (Fig. 3(d)). Therefore, the frequency response of (27) no longer corresponds to a first order low-pass response.

D. Full Up-CPO Frequency Response

As we explained in Section III-B, the carrier density dynamics $n_{e,\omega_{Pu}}$ are obtained from the pump-probe configuration and then used to determine the full frequency response of the Up-CPO configuration. Thereby, the power of Up-CPO responses, $p^c_{out,\omega_{c\pm d}}$, can be calculated by substituting the carrier density expressions (28)–(29) into (6)–(7):

$$p^c_{out,\omega_{c\pm d}} = -\frac{p^c_{in,1}}{4}\left(\frac{K_{n1n2}\bar{G}}{P^d_{sat,1}P^d_{sat,2}}T_{\pm}(\omega)\,p^d_{in,1}\right) \times\left(1-\frac{K_{n1n2}\overline{P^c_{in,1}}\bar{G}}{P^d_{sat,1}P^d_{sat,2}}\,T_{\pm}(\omega_c)\right) \tag{30}$$

with $T_{\pm}(\omega)=\frac{1\pm j\omega\tau_{d,12}}{(1\pm j\omega\tau_{d,1})(1\pm j\omega\tau_{d.2})}$, $T_{\pm}(\omega_c)=\frac{1\pm j\omega_c\tau_{d,12}}{(1\pm j\omega_c\tau_{d,1})(1\pm j\omega_c\tau_{d.2})}$, $P^d_{sat,\mathrm{i}}=\frac{wdW^d_p}{\Gamma a\tau_{e,i}}$ is the material saturation power at λ_d, W^d_p is the photon energy at the signal wavelength λ_d. Here $K^d_1=\frac{\overline{P^d_{in,1}}}{P^d_{sat,1}}\ \overline{G_1}$, $K^d_2=\frac{\overline{P^d_{in,1}}}{P^d_{sat,2}}\bar{G}$, $K_{n1n2}=P^d_{sat,2}K_{n1}+K_{n2}\overline{G_1}P^d_{sat,1}(1-K_{n1}(\frac{\overline{P^c_{in,1}}+\overline{P^d_{in,1}}}{P^d_{sat,1}}))$, $K_{n1}=\frac{\overline{G_1}-1}{(1+K^d_1)}$, and $K_{n2}=\frac{\overline{G_2}-1}{(1+K^d_2+K^c_2)}$.

IV. CALCULATION AND MEASUREMENT OF FREQUENCY RESPONSES FOR PUMP-PROBE AND UP-CPO SETUPS

In this section, we first give the experimental results in a pump-probe configuration in order to determine the value of $\tau_{d,12}$, $\tau_{d,1}$ and $\tau_{d,2}$ in (27) to (29). These parameters are then used in (30) to calculate and discuss the frequency response of signals generated by Up-CPO. Finally, we compare the calculation and the experimental results.

Three different SOAs have been measured: SOA-L, a device from InPhenix (IPSAD1502), SOA-NL and SOA-XN, from CIP Photonics. They are identified respectively as linear, nonlinear and extra nonlinear SOAs. The Table I represents the static characteristics of SOAs measured at the maximum biasing current and at −25 dBm input optical power.

TABLE II
CUTOFF FREQUENCY OF SOA-L (GHZ)

	0dB	5dB	10dB
f_{12}	0.81	1.46	2.17
f_1	0.5	1.03	1.82
f_2	1.62	2.7	5.33
f_{3dB}	0.76	1.63	3.95

A. Pump-Probe Characterization

For the experimental pump-probe setup, an intensity-modulated optical pump of 5 dBm at $\lambda_{Pu}=1545$ nm and a continuous wave (CW) optical probe of −5 dBm at $\lambda_{Pr}=1550$ nm are simultaneously injected into the SOA. An optical filter is used at the SOA output to measure the signal converted at λ_{Pr} through XGM. After photodetection, we measure the RF signal $p^{Pr}_{out,\ \omega_{Pu}}$ by a vector network analyzer (VNA). As each SOA device is different, the measurements are made with respect to the static optical gains 0 dB, 5 dB and 10 dB, in presence of the input pump power of 5 dBm and the input probe power of −5 dBm, to make comparisons possible.

Fig. 4(a), 4(b) and 4(c) show, in dotted line, the calculated data of the normalized frequency low-pass response of the measured RF power $p^{Pr}_{out,\omega_{Pu}}$ for the three SOAs. The experimental results, in solid line, show that for the SOAs NL and XN the RF power presents a large bandwidth, measured at −3 dB, which can reach 18.45 GHz, while for SOA-L a bandwidth limited to 3.95 GHz is obtained for gain 10 dB. We also notice that non-flat responses are obtained for SOAs NL and XN.

In order to determine the value of $\tau_{d,12}$, $\tau_{d,1}$ and $\tau_{d,2}$ in (27) to (29) we fit the experimental results of the pump-probe configuration by the normalized form of the measured RF power $p^{Pr}_{out,\omega_{Pu}}$ for SOA-L, SOA-NL and SOA-XN. The normalized function is obtained from (27) as:

$$T(f)=\frac{1+j\omega\tau_{d,12}}{(1+j\omega\tau_{d,1})(1+j\omega\tau_{d,2})}=\frac{1+j\frac{f}{f_{12}}}{\left(1+j\frac{f}{f_1}\right)\left(1+j\frac{f}{f_2}\right)} \tag{31}$$

where f_t is the cutoff frequency for each $1+j\frac{f}{f_t}$ term with $f_t=\frac{1}{2\pi\tau_{d,t}}$ and $t=12$, 1 and 2. The obtained value of $f_{d,12}$, $f_{d,1}$ and $f_{d,2}$ for the three SOAs are shown in Table II, Table III and Table IV, respectively.

The calculated data of the normalized RF power from $p^{Pr}_{out,\omega_{Pu}}$ show a good agreement with the measured ones (Fig. 4) for the three different SOAs. These show that the SOA

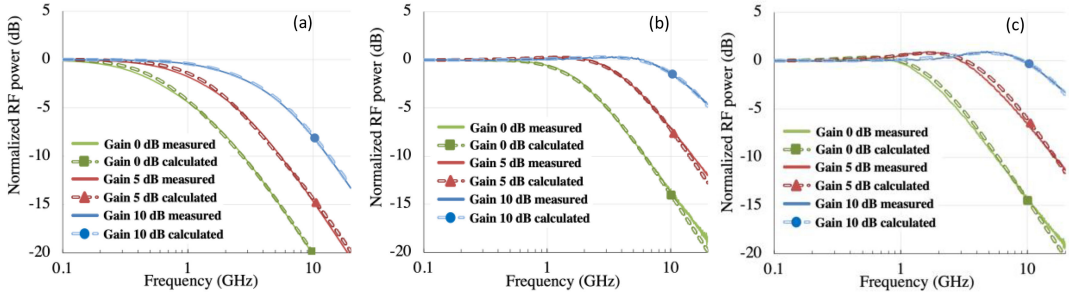

Fig. 4. Normalized RF power for: SOA-L (a), SOA-NL (b) and SOA-XN (a). Calculated data are in dotted line and measured ones are in solid line.

TABLE III
CUTOFF FREQUENCY OF SOA-NL (GHZ)

	0dB	5dB	10dB
f_{12}	0.6	1.26	2.5
f_1	0.64	1.5	2.8
f_2	1.91	4	12
f_{3dB}	2.14	5.23	14.65

TABLE IV
CUTOFF FREQUENCY OF SOA-XN (GHZ)

	0dB	5dB	10dB
f_{12}	0.6	1.3	3.37
f_1	0.8	1.8	4.43
f_2	1.45	3.9	12
f_{3dB}	2.24	5.97	18.45

modeling by dividing its length into two sections allows us to reproduce their high-order frequency responses with a good accuracy. Moreover, the fitting results show that a flat frequency response in the bandwidth at -3 dB is obtained when $f_{12} \geq f_1$, corresponding to $\tau_{d,12} \leq \tau_{d,1}$. Otherwise, a slight overshoot appears as for SOAs NL and XN at gains 5 dB and 10 dB, that corresponds to $\tau_{d,12} > \tau_{d,1}$, where (27) no longer has a first-order low-pass response (as stated in Section III-C).

4.2 Calculation of Absolute Frequency Response for Up-CPO Setup

For practical reasons, in experimental measurements, we only have an easy access to relative responses, i.e., the difference between two measurements, rather than the absolute ones. The absolute amplitude and phase responses of Up-CPO signals can be calculated by substituting the normalized function (31) of the calculated f_t in Tables II, III and IV into (30). $p^c_{out,\omega_{c\pm d}}$ can be written as:

$$p^c_{out,\omega_{c\pm d}} = -\frac{p^c_{in,1}}{4}\left(\frac{K_{n1n2}\bar{G}}{P^d_{sat,1}P^d_{sat,2}}T_{\pm}(f)\,p^d_{in,1}\right) \times\left(1-\frac{K_{n1n2}\overline{P^c_{in,1}}\bar{G}}{P^d_{sat,1}P^d_{sat,2}}\,T_{\pm}(f_c)\right) \tag{32}$$

The resulting $p^c_{out,\omega_{c\pm d}}$ can be rewritten as follows:

$$p^c_{out,\omega_{c\pm d}} = -\frac{A}{4m}p^d_{in,1}T_{\pm}(f)\left(1-A\,T_{\pm}(f_c)\right) \tag{33}$$

where $A = \frac{K_{n1n2}\overline{P^c_{in,1}}}{P^d_{sat,1}P^d_{sat,2}}\bar{G}$ is a constant for an operating point and $m = \frac{p^c_{in,1}}{\overline{P^c_{in,1}}}$ is the modulation index of the optical input signal at λ_c. We vary f in a range of 5 GHz around f_c with $f = f_c \pm f_d$.

The power, in dBm, and the phase of $p^c_{out,\omega_{c\pm d}}$ for an operating of gain G of the SOA can be written form (33) as:

$$\left|p^c_{out,\omega_{c\pm d}}\right|_G\ (dBm) = B_G + 10log\left|T_{\pm}(f)\right| \tag{34}$$

$$arg\left(p^c_{out,\omega_{c\pm d}}\right)\Big|_G = \pi + C_G + arg\left(T_{\pm}(f)\right) + arg\left(p^d_{in,1}\right) - arg\left(p^c_{in,1}\right) \tag{35}$$

where B_G and C_G are constant terms with:

$$B_G = 10log\frac{A}{4m}\frac{p^d_{in,1}}{10^{-3}}\left|1-A\,T_{\pm}(f_c)\right| \tag{36}$$

$$C_G = arg\left(1-A\,T_{\pm}(f_c)\right) \tag{37}$$

The Up-CPO technique operates as a frequency up-conversion function where the responses of the pump-probe configuration are shifted around f_c. The phase response (35) is governed directly by $arg(T_{\pm}(f))$ which presents a maximum variation range of 180°. For a given frequency interval, the phase shift variation range depends on the dynamic carrier lifetimes $\tau_{d,12}$, $\tau_{d,1}$ and $\tau_{d,2}$. Equations (28) and (29) show that the phase shift can be adjusted by the injected optical power and/or the bias current.

In Fig. 5, we normalized the power and the phase of $p^c_{out,\omega_{c\pm d}}$ to be null at $f = f_c$. The calculation is done in a bandwidth range of 5 GHz around f_c.

As we have seen in Sections III-C and IV-A, SOA-L has a first-order low pass response (Fig. 4(a)) shown in Fig. 5(a), 5(c), and 5(e). The phase variation is almost linear over a 1 GHz frequency range. However, for nonlinear SOAs with a large XGM bandwidth, a nonlinear phase response appears as for SOAs NL and XN at gains 5 dB and 10 dB (see Fig. 5(a), 5(c), and 5(e)). This corresponds to $\tau_{d,12} > \tau_{d,1}$ (Fig.3 (d)), where (27) has no longer a first-order low-pass response (Fig. 4(b-c)). We can see that the obtained phase responses present non linearities that limit the phase variation bandwidth. This limitation could be addressed by adding a predistortion block to the system.

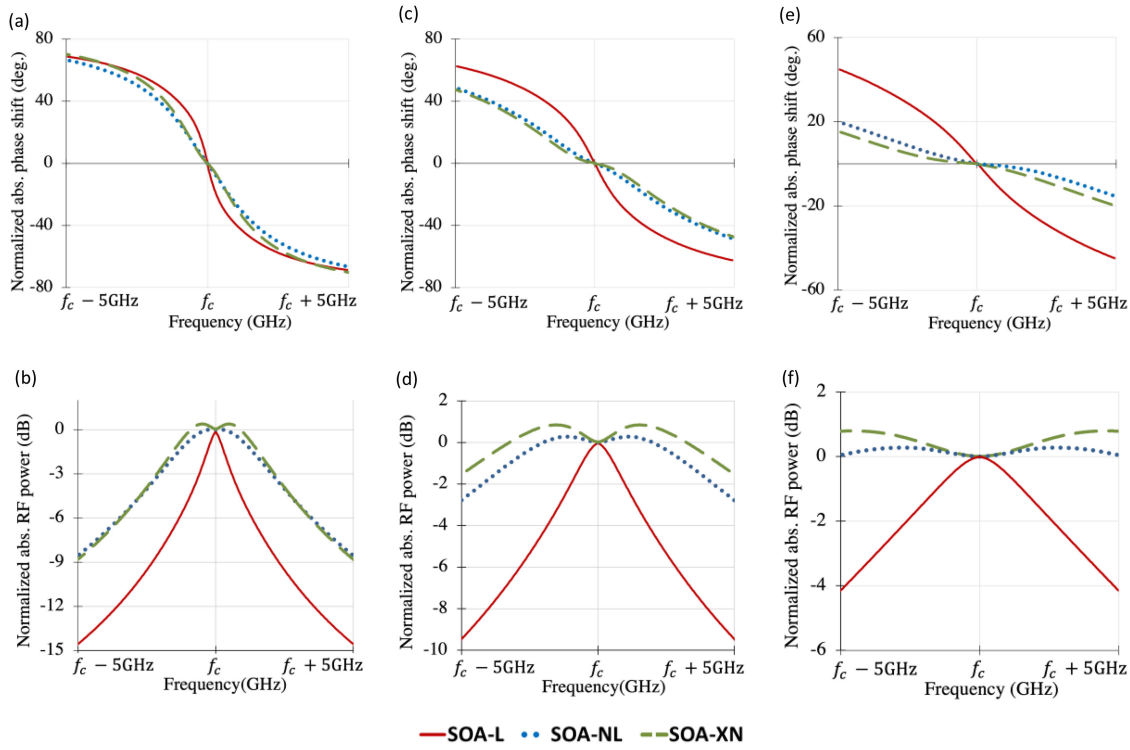

Fig. 5. Normalized absolute phase shift for the three SOAs at the gain: 0 dB (a), 5 dB (c) and 10 dB (e). Normalized absolute RF power for the three SOAs at the gain: 0 dB (b), 5 dB (d) and 10 dB (f).

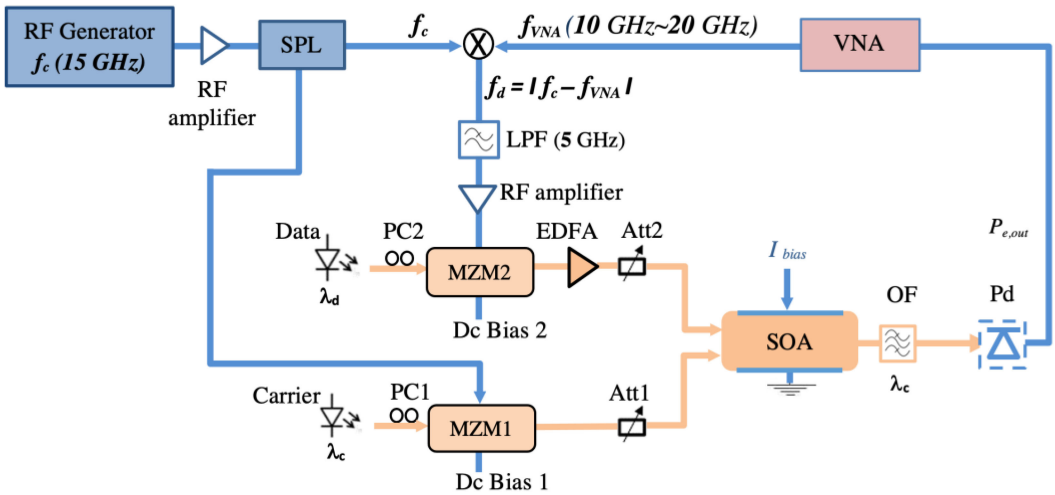

Fig. 6. Experimental setup for Up-CPO measurements induced by slow and fast light effects and XGM in a SOA. PC1 and PC2: Polarization Controller, Pd: Photodetector, EDFA: Erbium-doped fiber amplifier, LPF: RF low-pass filter, SPL: RF Splitter.

For an optical gain equal to 0 dB, all the three SOAs present a high phase shift and a high power variation (Fig. 5(a), 5(b)) due to their limited bandwidth, less than 2.24 GHz (Tables II to IV). By increasing the SOA gain to 5 dB and 10 dB, SOA-L always shows larger phase shifts and power variations than the ones of SOA-NL and XN (Fig. 5(c), 5(d), 5(e) and 5(f)) due to their higher cutoff frequencies (Tables III to V).

In addition, we note that the overshoot existing for both SOA-NL and XN at gains 5 dB and 10 dB in Fig. 4 also appears for the normalized absolute amplitude responses in Fig. 5(b), 5(d) and 5(f), due to $f_1 \geq f_{21}$ as seen in Section IV-A.

C. Validation of Small-Signal Calculations By Measurement of Frequency Responses for Up-CPO Setup

The experimental setup is illustrated in Fig. 6. A first optical signal emitted at $\lambda_c = 1550$ nm is intensity-modulated at a high radiofrequency $f_c = 15$ GHz via the Mach-Zehnder modulator MZM1. A second optical signal emitted at $\lambda_d = 1545$ nm is intensity-modulated via the Mach-Zehnder modulator MZM2 at a low RF frequency f_d varying from 0.1 to 5 GHz. It is generated, by using an RF mixer, as the difference between f_c and f_{VNA}, a signal varying from 10 to 20 GHz, generated by the VNA.

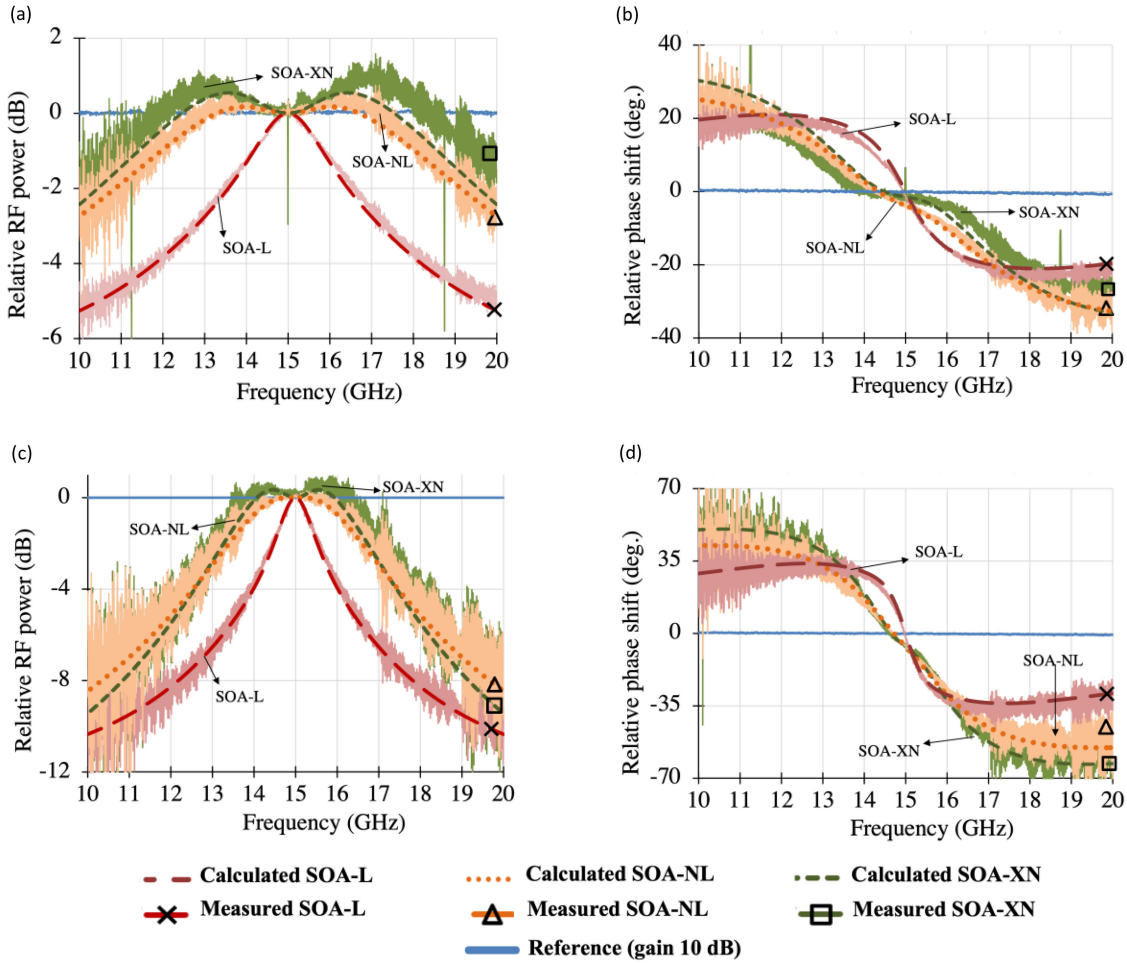

Fig. 7. Measured and calculated results for a gain of 5 dB with a reference gain of 10 dB: (a) relative RF amplitude for SOA-L, SOA-NL and SOA-XN, (b) relative phase shift for SOA-L, SOA-NL and SOA-XN. Measured and calculated results for a gain of 0 dB with a reference gain of 10 dB: (c) relative RF amplitude for SOA-L, SOA-NL and SOA-XN, (d) relative phase shift for SOA-L, SOA-NL and SOA-XN. Calculated data are in dotted line, and measured data are in solid line.

The laser wavelengths are close to the one for which the gain of SOAs is maximum. An EDFA amplifies the modulated input data signal P_{in}^{d}. At the SOA output, an optical filter OF with an optical bandwidth of about 0.4 nm is set at λ_c. The optical mean powers $\overline{P_{in}^{c}}$ and $\overline{P_{in}^{d}}$ are adjusted by the optical attenuators Att1 and Att2, respectively at -5 and 5 dBm. After the photodiode Pd, the magnitude and the phase shift of the RF signal $P_{e,\,out}$ are measured by a VNA at different static optical gains for each SOA device.

The measurements of amplitude and phase shift are evaluated relatively to a reference that is the frequency response at the gain of 10 dB. The operating frequency is fixed at $f_c = 15$ GHz. It could be largely higher, but it was fixed at this value due to our experimental setup limitations. It should be noted that the used frequency $f_c = 15$ GHz for the SOA-NL and SOA-XN, is below their cutoff frequency for gain 10 dB (Tables III and IV).

The experimental results of the relative phase shift and the normalized relative amplitude of the Up-CPO signal are shown in Fig. 7 for gains 0 dB and 5 dB. We can see that the measured phase shift presents an offset at 15 GHz for both SOA-NL and SOA-XN. This is due to the large bandwidth of the reference response at gain 10 dB, where $f_{3dB} = 18.45$ GHz for SOA-XN and 14.65 GHz for SOA-NL (see Tables III and IV), which is close to or higher than f_c. For the gain 5 dB, the cutoff frequency for SOA-XN (5.97 GHz) and for SOA-NL (5.23 GHz) are not significantly lower than f_c. Thus, the frequency response of Up-CPO at $\omega_{c\pm d}$ depends on both n_{e,ω_d} and n_{e,ω_c}, as described in Section III-A.

The calculation of the relative amplitude and relative phase responses of Up-CPO are performed by using (34) and (35) and are then normalized at the frequency f_c. Fig. 7 shows a good agreement over all the 10 GHz measurement range around f_c for SOA-L between the theoretical (in dotted line) and experimental results (solid lines) for gains 0 dB (Fig.7.a-b) and 5 dB (Fig.7.c-d) of the relative amplitude and relative phase shift where the SOA bandwidth is always lower than f_c.

For SOA-NL and SOA-XN, frequency responses for the reference chosen at the gain 10 dB present a cutoff frequency close to (for SOA-NL) or slightly above (for SOA-XN) f_c. Although that the approximations concerning the beating terms inside the SOA (that were discussed in Section III-B) are relatively rough in this case, the relative Up-CPO responses respectively for gains 0 and

5 dB show a good agreement over all the 10 GHz measurement range around f_c except for the responses of SOA-XN for gain 5 dB (Fig. 7.a-b) where a difference appears between theoretical and experimental results.

V. Conclusion

We have presented, for three different SOAs, which bandwidths range from 0.76 to 18.45 GHz, theoretical and experimental analysis of an Up-CPO. A tunable phase shift has been obtained with more than 1 GHz of instantaneous bandwidth at an operating frequency of 15 GHz, with a maximum phase shift of 90° (for SOA-XN). We demonstrated that modeling SOAs by two sections is sufficient, both for linear and nonlinear SOAs, with a good agreement between theoretical and experimental results.

Acknowledgment

This research is supported by the Brittany Region (France) through an ARED project and the Université de Bretagne Occidentale (UBO). It is part of a joint Ph.D. thesis supervision between UBO and the École Nationale d'Ingénieurs de Brest (ENIB).

References

[1] J. Capmany and D. Novak, "Microwave photonics combines two worlds," *Nature Photon.*, vol. 1, no. 6, 2007, Art. no. 319.

[2] R. A. Minasian *et al.*, "Microwave photonic signal processing," *Opt. Exp.*, vol. 21, no. 19, pp. 22918–22936, Sep. 2013.

[3] S. Pan, X. Ye, Y. Zhang, and F. Zhang, "Microwave photonic array radars," *IEEE J. Microw.*, vol. 1, no. 1, pp. 176–190, Jan. 2021.

[4] J. Mørk, R. Kjær, M. van der Poel, and K. Yvind, "Slow light in a semiconductor waveguide at gigahertz frequencies," *Opt. Exp.*, vol. 13, no. 20, pp. 8136–8145, 2005.

[5] S. Sales, W. Xue, J. Mork, and I. Gasulla, "Slow and fast light effects and their applications to microwave photonics using semiconductor optical amplifiers," *IEEE Trans. Microw. Theory Tech.*, vol. 58, no. 11, pp. 3022–3038, 2010.

[6] C. J. Chang-Hasnain and S. L. Chuang, "Slow and fast light in semiconductor quantum-well and quantum-dot devices," *J. Lightw. Technol.*, vol. 24, no. 12, pp. 4642–4654, Dec. 2006.

[7] P. Berger, J. Bourderionnet, D. Dolfi, F. Bretenaker, and M. Alouini, "Slow and fast light in semiconductor optical amplifiers for microwave photonics applications," in *Adv. Opt. Amplifiers*, INTECH, vol. 9, 2011, pp. 179–204.

[8] W. Xue and J. Mørk, "Tunable true-time delay of a microwave photonic signal realized by cross gain modulation in a semiconductor waveguide," *Appl. Phys. Lett.*, vol. 99, no. 23, 2011, Art. no. 231102.

[9] N. Hamdash, A. Sharaiha, T. Rampone, C. Quendo, N. Martin, and D. L. Berre, "Optically controlled RF phase shifts in SOAs by adding the XGM response of an optical signal," *IEEE Photon. Technol. Lett.*, vol. 31, no. 13, pp. 1060–1063, Jul. 2019.

[10] N. Hamdash *et al.*, "Experimental and small-signal analysis of microwave photonic phase shifter based on slow and fast light using linear and nonlinear semiconductor optical amplifiers," in *Proc. IEEE Int. Topical Meeting Microw. Photon.*, Toulouse, France, 2018, pp. 1–4.

[11] P. Berger, J. Bourderionnet, F. Bretenaker, D. Dolfi, and M. Alouini, "Time delay generation at high frequency using SOA based slow and fast light," *Opt. Exp.*, vol. 19, no. 22, pp. 21180–21188, 2011.

[12] G. P. Agrawal, "Population pulsations and nondegenerate four-wave mixing in semiconductor lasers and amplifiers," *J. Opt. Soc. Amer. B*, vol. 5, pp. 147–159, Jan. 1988.

[13] M. J. Connelly, "Wideband semiconductor optical amplifier steady- state numerical model," *IEEE J. Quantum Electron.*, vol. 37, no. 3, pp. 439–447, Mar. 2001.

[14] S. Chin *et al.*, "Broadband true time delay for microwave signal processing, using slow light based on stimulated brillouin scattering in optical fibers," *Opt. Exp.*, vol. 18, no. 21, pp. 22599–22613, 2010.

[15] S. O. Duill, E. Shumakher, and G. Eisenstein, "On the role of high-order coherent population oscillations in slow and fast light propagation using semiconductor optical amplifiers," *IEEE J. Sel. Topics Quantum Electron.*, vol. 15, no. 3, pp. 578–584, May/Jun. 2009.

[16] P. Morel and A. Sharaiha, "Wideband time-domain transfer matrix model equivalent circuit for short pulse propagation in semiconductor optical amplifiers," *IEEE J. Quantum Electron.*, vol. 45, no. 2, pp. 103–116, Feb. 2009.

[17] C. Bohemond, T. Rampone, and A. Sharaiha, "Performances of a photonic microwave mixer based on cross-gain modulation in a semiconductor optical amplifier," *J. Lightw. Technol.*, vol. 29, no. 16, pp. 2402–2409, Aug. 2011.

[18] B. Cabon, J. Chazelas, and D. Dolfi, "Microwave optoelectronics - Modulation, links and switching," *Techn. de l'ingénieur. Electronique*, vol. 4, no. E3331, pp. E3331.1–E3E3331, 2003.

[19] P. P. Baveja, A. M. Kaplan, D. N. Maywar, and G. P. Agrawal, "Pulse amplification in semiconductor optical amplifiers with ultrafast gain-recovery times," *Proc. SPIE*, vol. 7598, 2010, Art. no. 759817.

[20] V. Agrawal and M. Agrawal, "Characterization and optimization of semiconductor optical amplifier for ultra high speed applications: A review," in *Proc. Conf. Signal Process. Commun. Eng. Syst.*, Vijayawada, India, 2018, pp. 215–218.

[21] M. J. Connelly, *Semiconductor Optical Amplifiers*, Berlin, Germany: Springer, 2007.